Nanoscale

Accepted Manuscript

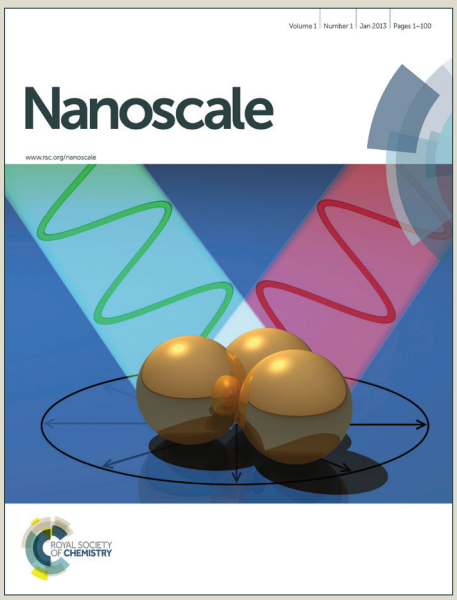

ROYAL SOCIETY OF CHEMISTRY

www.rsc.org/nanoscale

Fabrication of Large Scale Single Crystal Bismuth Telluride (Bi_2Te_3) Nanosheet Arrays by Single Step Electrolysis Process

Hung-Wei Tsai,[1]Tsang-Hsiu Wang,[1]Tsung-Cheng Chan,[1]Pei-Ju Chen,[2]Chih-Chun Chung,[1] Alireza Yaghoubi[3], Chien-Neng Liao,[1]Eric Wei-Guang Dia[2], and [1]Yu-Lun Chueh[1,4]*

[1]Department of Materials Science and Engineering, National Tsing Hua University, Hsinchu, 30013, Taiwan

[2] Department of Applied Chemistry, National Chiao Tung University, Hsinchu 30010, Taiwan

[3]Centre for High Impact Research, University of Malaya, Kuala Lumpur 50603, Malaysia.

[4]Center for Nanotechnology, Material Science, and Microsystem, National Tsing Hua University, Hsinchu, 30013, Taiwan

*E-mail:ylchueh@mx.nthu.edu.tw

Abstract- Nanolizing of the thermoelectric materials is one approach to reduce the thermal conductivity and hence enhances the figure of merit. Bismuth telluride (Bi_2Te_3) based materials have excellent figure of merit at room temperature. For device applications, precise control and fast fabrication for the nanostructure of thermoelectric materials are essential issues. In present study, we demonstrate one-step electrolysis process to directly form Bi_2Te_3 nanosheet arrays (NSAs) on the surface of Bi_2Te_3 bulk with controllable spacing distance and depth by tuning the applied bias and duration. The single sheet of NSAs reveals that the average thickness and electrical resistivity of single crystalline Bi_2Te_3 in composition are 399.8 nm and 137.34 μΩ-m, respectively. The formation mechanism of NSAs has been proposed. A 1.12 % efficiency of quantum-dot-sensitized solar cells with Bi_2Te_3 NSAs for counter electrode has been demonstrated, indicating that Bi_2Te_3 NSAs from top-down process with high ratio of surface area to volume show a promising candidate for possible applications such as thermoelectrics, dye-sensitized solar cells (DSSCs), and lithium-ion batteries.

Keywords: bismuth telluride, Nanosheet Arrays, Electrolysis Process

1. **Introduction**

Two-dimensional materials[1] have the van der Waals gap in their crystal structure such as graphite[2], h-BN[3], MoS_2[4], and Bi_2Te_3.[5] Because of the weak van der Waals force, two-dimensional materials can be exfoliated to nanosheets by mechanical cleavage methods. Besides, metal ions can be intercalated into the van der Waals gap of these two-dimensional materials and thus form nanosheets.[6] In recent years, Bi_2Te_3 based materials have attracted much attention due to their interesting physical properties. For example, nanostructured Bi_2Te_3 with high surface area has been used for dye-sensitized solar cells (DSSCs)[7] and lithium-ion batteries.[8] In addition, nanostructured Bi_2Te_3 comes with a high thermoelectric figure of merit, namely ZT value, which is used to examine the thermoelectric performance of a thermoelectric material.[9] The dimensionless figure of merit (ZT) can be given by $ZT = (S^2\sigma/\kappa)T$ where S, σ, κ, and T are Seebeck coefficient (μVK^{-1}), electrical conductivity ($\Omega^{-1}m^{-1}$), thermal conductivity ($Wm^{-1}K^{-1}$), and temperature (K) respectively. The ZT value of the nanostructured thermoelectric materials can be enhanced as thermal conductivity decreases as reported by both experimental[10] and theoretical[11] works. Therefore, it is an important issue to control the nanostructure of thermoelectric materials precisely.

The quintuple layer (QL) of the Bi_2Te_3 consists of five monoatomic sheets ($Te^{(1)}$-Bi-$Te^{(2)}$-Bi-$Te^{(1)}$), which is obtained by mechanical exfoliation or metal ion intercalation. The significantly decreased thermal conductivity of the QL of the Bi_2Te_3 was observed.[12] For high production yield and size uniformity of Bi_2Te_3 nanosheets, hydrothermal synthesis and electrochemical method are suitable methods for mass production.[9,13] Although, nanoplates, nanowires, nanotubes, and nanodots could be obtained by a hydrothermal method, a complicated device fabrication process, is needed. In contrast to the hydrothermal method, electrochemical method is a prior way to achieve mass production for thermoelectric device applications. For example, a large area of arranged Bi_2Te_3 nanowires was obtained by electrodepositing Bi_2Te_3 into an anodic aluminum oxide (AAO) template with enhanced thermoelectric properties.[13] However, post-treatments such as removal of AAO or transfer process of arranged Bi_2Te_3 NWs for device applications may be needed.

To the best of our knowledge, fast fabrication of a large scale Bi_2Te_3 nanostructure has not yet been explored. The electrochemical method is a non-vacuum process and comes with advantages of

large scale and low-cost fabrication. In this regard, we demonstrate one-step electrochemical method to fabricate large scale single crystal Bi_2Te_3 nanosheet arrays (NSAs) on the surface of Bi_2Te_3 bulk. We have found that the area of Bi_2Te_3 NSAs depends on the plane directions of Bi_2Te_3 grains and the depth of Bi_2Te_3 NSAs relys on the applied bias and duration. Phase and microstructures were characterized by X-ray diffractometer, Raman spectrometer, and transmission electron microscopy (TEM). In addition, the physical properties, such as thickness and resistivity of single Bi_2Te_3 nanosheet were measured and investigated in detail. The formation mechanism of NSAs has been proposed. Finally, the possible replacement of counter electrode for DSSC has been demonstrated.

2. Experimental Section

Fabrication of Bi_2Te_3 NSAs:

Bismuth (99.99 wt. %, ADMAT) and tellurium (99.999 wt. %, ADMAT) were used without further purification. Dilute nitric acid with pH level of 1.2 was used as electrolyte in one-step electrochemical method with three electrodes system for bias control. Because of compensation for evaporation of Te at high-temperature process, additional Te (3 wt. %) was added for synthesis of stoichiometry Bi_2Te_3 compound. The weighed Bi and Te ingots were sealed in an evacuated quartz tube and annealed in a furnace at 850 ^oC for 48 h for synthesis of Bi_2Te_3 bulk. Subsequently, the synthesized Bi_2Te_3 bulk were sliced into circular disks with 1 cm in diameter and 3 mm in thickness. The polished Bi_2Te_3 bulk was used as working electrode where the mercury/mercury chloride (Hg/Hg_2Cl_2) electrode and platinum electrode were used as reference electrode and counter electrode, respectively. The Bi_2Te_3 NSAs with a periodic spacing distance of ~1 μm and tens of micrometers in depth were formed while various biases have been applied for few seconds to few minutes.

Devices fabrication:

For the electrical measurements, the Bi_2Te_3 nanosheet was put on a 50 nm-thick SiO_2/Si substrate, followed by dropping the sample into diluted nitric acid to remove the native oxide. 150 nm-thick Ni metal was deposited by electron beam deposition as electrodes and defined by photolithography process. For the CdSe QD-SSCs fabrication, the TiO_2 films were prepared by screen printing of TiO_2 paste on FTO glass and sintered to form TiO_2 mesoporous. Chemical bath deposition was used to

assemble CdSe QDs onto the TiO_2 electrode and then the TiO_2/CdSe electrode was sandwiched with Bi_2Te_3 NSAs, pure FTO, and Pt as counter electrodes for further photovotaic properties measurements after injecting the polysulfide as electrolyte. The active area of the cell was 0.16 cm^2.

Characterization :

The crystallization and compositions of Bi_2Te_3 are confirmed by X-ray diffraction (Shimadzu XRD 6000, Cu Kα radiation with wavelength of 0.154 nm) and micro-Raman spectrometer (632.8 nm He-Ne laser with laser intensity of 2 mW). Scanning electron microscopy (JSM 6500-F, JOEL operated at 15 kV with resolution of 3.0 nm) and field-emission transmission electron microscopy (JEM-3000F, JEOL operated at 300 kV with point-to-point resolution of 0.17 nm) were used to obtain the microstructures and the compositions. The electrical properties were measured using a Agilent B1500A semiconductor parameter analyzer at room temperature.

3. Results and Discussion

Figure 1 shows schematics of how we fabricate Bi_2Te_3 NSAs with a periodic spacing distance of ~1 μm and tens of micrometers in depth at various biases for few seconds to few minutes. Bi_2Te_3 bulk was first prepared by sintering of Bi and Te powders together and then as-prepared Bi_2Te_3 bulk was polished until the surface appears metallic luster as shown in Figure 1(a). Figure 1 (b) shows the schematics of three electrode system, which is used to fabricate Bi_2Te_3 NSAs. The polished Bi_2Te_3 bulk was used as working electrode. The mercury/mercury chloride (Hg/Hg_2Cl_2) electrode and platinum electrode were used as reference electrode and counter electrode, respectively. After applying a negative bias on the working electrode, Bi_2Te_3 NSAs were formed on the surface of Bi_2Te_3 bulk as shown in Figure 1 (c). The corresponding scanning electron microscopy (SEM) image is depicted in Figure 1 (d), in which we could observe Bi_2Te_3 NSAs formed on the allowed plane direction grains in upper part and lower-left part. Note that no Bi_2Te_3 NSAs were formed on the forbidden plane direction grains in lower-right part. Inset shows a higher magnification image of single Bi_2Te_3 layer captured from the rectangular area in Figure 1(d).

After the electrochemical treatment, the Bi_2Te_3 bulk was immersed in deionized water to get rid of the electrolyte. The Bi_2Te_3 NSAs is coincident with rhombohedral Bi_2Te_3 (JCPDS 89-4302) in XRD spectrum as well as the Bi_2Te_3 bulk without formation of NSAs as shown in Figure 2 (a). Moreover,

the single Bi_2Te_3 sheet has been examined by using direct sonication of Bi_2Te_3 NSAs in ethanol for comparison. The corresponding Raman spectra and transmission electron microscopy (TEM) image of the single Bi_2Te_3 sheet were shown in Figures 2(b)-2(d), respectively. For the Raman spectra of a single Bi_2Te_3 sheet, two main peaks at 102.4 and 133.2 cm^{-1} were observed, which are attributed to optical modes of $2E_g$ and $2A_{1g}$, respectively.[14] These two main optical mode peaks are consistent with the Raman spectra of the pristine Bi_2Te_3 bulk (Figure 2 b). The Figure 2 (c) shows a TEM image of a Bi_2Te_3 sheet. The dark lines observed in the Bi2Te3 sheet are probably due to the dislocations inside. Inset in the Figure 2(c) shows the corresponding selected area diffraction pattern (SAD). Obviously, symmetric spots indicate a single crystalline feature of the Bi_2Te_3 sheet. According to zone axis of electron diffraction pattern, the plane direction of Bi_2Te_3 sheet is (001), which is very important for understanding the formation mechanism of Bi_2Te_3 NSAs. The high resolution TEM (HRTEM) image as shown in Figure 2(d) is in agreement with the Bi_2Te_3 (110) plane where lattice spacing of 0.218 nm was indexed.

Figure 3 (a) shows that the unit cell of the Bi_2Te_3 is consisted of fifteen monoatomic sheets of bismuth and tellurium atoms in the rhombohedral crystal structure. The bonding states between Bi-$Te^{(1)}$ and Bi- $Te^{(2)}$ are different and are attributed to ionic and covalent bonds, respectively. It is reported by Drabble and Goodman that these bonds are much stronger than the Van der Waals force ($Te^{(1)}$-$Te^{(1)}$).[15] To shed light on the formation mechanism of the Bi_2Te_3 NSAs, the *ex-situ* formation of Bi_2Te_3 NSAs was observed at the applied bias of -2V with different duration from 5, 15, and 30 sec as shown in Figure 3(b), respectively. The corresponding schematics of formation processes of Bi_2Te_3 NSAs are also shown in Figure 3 (c). With increasing of duration, the Bi_2Te_3 bulk was etched away and forms Bi_2Te_3 NSAs during the electrolysis process. The reactivity sites of Bi_2Te_3 under applied bias can be examined by the Bi-Te bond energy. Kaviany and co-workers reported the bond energies of $Te^{(1)}$-Bi, $Te^{(2)}$-Bi, and $Te^{(1)}$- $Te^{(1)}$ in Bi_2Te_3 to be 0.974, 0.5801, and 0.0691 eV by using computational methods, respectively.[16] As seen in the Figure 3(a), a $Te^{(1)}$ atom binds with three Bi and three $Te^{(1)}$ atoms. As a result, it needs 3.1293 eV to the release a $Te^{(1)}$ atom (Detailed calculation, please see the supplementary information). For a $Te^{(2)}$ atom binds with six Bi atoms, it needs 3.4806 eV to release a $Te^{(2)}$ atom (Detailed calculation, please see the supplementary information). However,

it needs 4.6623 eV to release a Bi atom from three Bi-$Te^{(1)}$ bonds and three Bi-$Te^{(2)}$ bonds (Detailed calculation, please see the supplementary information). Therefore, the $Te^{(1)}$ atom is the easiest to be removed because of its weak bonding energy. Besides, the distance between two monoatomic sheets of $Te^{(1)}$-$Te^{(1)}$ is 2.598 Å and the diameter of hydrogen atom can be considered as two times of Bohr radius (1.058 Å), which is smaller than the gap of the $Te^{(1)}$-$Te^{(1)}$.[17] Therefore, hydrogen ions can be easily inserted into the gap of the $Te^{(1)}$-$Te^{(1)}$ and thus react with $Te^{(1)}$ atoms to reduce H_2 and H_2Te gases during the electrolysis process. For better understanding, we design an experiment to prove the existence of H_2Te gas by observing the H_2Te derived tellurium blade on the surface of suspended silicon substrate (details in Supporting Information). Once $Te^{(1)}$ atoms are etched, the Bi_2Te_3 NSAs can be formed along the (001) surface of the Bi_2Te_3 bulk. The etching processes of Bi_2Te_3 are shown in Figure 3 (c).

To understand the spacing control of the Bi_2Te_3 NSAs, the different biased were applied, for which the total charge flux for each applied bias was fixed. The spacing distances of Bi_2Te_3 NSAs as the function of various applied biases were plotted as shown in Figure 4 (a). The electrolysis parameters and SEM images of the Bi_2Te_3 NSAs for various applied biases are shown in Table 1 and Figures 4 (b) to (f), respectively. Obviously, the spacing distance is slightly decreased as the applied bias increases, suggesting that more number of reaction sites are created under the larger applied bias. The corresponding relation between spacing distance and applied bias could be described by fitted curve as below:

$$y=-0.161\times ln(-x)+1.4333$$

Where y is the spacing distance and x is the applied bias. To measure electrical properties of Bi_2Te_3 nanosheet, conventional photolithography technique was used to prepare the two-terminal devices and the corresponding thicknesses of the Bi_2Te_3 nanosheet was measured by atomic force microscopy (AFM). Then, the measured thickness of the Bi_2Te_3 nanosheet was used for resistivity calculation as shown in Figure 5. Inset shows the corresponding device configuration. Consequently, the average thickness and electrical resistivity of the Bi_2Te_3 nanosheet are ~399.8 nm and ~137.34 μΩ-m, respectively. The electrical resisitivity of the Bi_2Te_3 nanosheet is larger than that in a previous work[18] by one order of magnitude, which may result from the contact resistance owing to two-terminal

measurement and doping condition during synthesis of Bi_2Te_3.[19] These two reasons can result an increasing in the measured resistance of the Bi_2Te_3 nanosheet.

Generally, plantinum (Pt) is used as a counter electrode for quantum-dot-sensitized solar cells (QD-SSCs). However, Pt is an expensive and rare material in the world. Some alternative materials for counter electrode have been proposed such as metal chalcogenide[20,21], Au[22], and carbon[23]. The metallic property due to very low band gap of ~0.15 eV[24] and matched electron affinity of ~4.125-4.525 eV[25] makes Bi_2Te_3 NSAs a potential candidate as the counter electrode to replace Pt for possible application in QD-SSCs. To shed on this part, Figure (6) shows the current density-voltage (J-V) curves of a CdSe QD-SSCs with Bi_2Te_3 NSAs, pure FTO, and Pt as counter electrodes under 1 sun illumination. The photovoltaic (PV) properties of these electrodes are listed in Table 2. As can be seen in the Table 2, the open-circuit voltage (V_{oc}) of the Bi_2Te_3 counter electrode is 0.581 V, which is lower than the Pt electrode by 0.035 V. The short-circuit current (J_{sc}) of the Bi_2Te_3 NSAs and Pt counter electrodes are 6.891 and 7.314 mA/cm^2, respectively. Therefore, the PV conversion efficiency of the Bi_2Te_3 NSAs as the counter electrode can be reached to 1.12 %, which is better than that of the device using pure FTO as the electrode (0.18 %) and is comparable with that of Pt as counter electrodes (0.9~1.84 %).

4 Conclusions

We have demonstrated a novel one-step electrolysis process for directly fabricating large scale Bi_2Te_3 NSAs. The composition and properties of Bi_2Te_3 NSAs have been analyzed by XRD, Raman, SEM, TEM, and electrical measurements. The spacing distance and depth of Bi_2Te_3 NSAs depend on applied bias, current desities and bias duration. Our experimental results indicate that the spacing distance of Bi_2Te_3 nanosheets is of 1 μm with thickness of several hundred nanometers. Moreover, the Bi_2Te_3 NSAs show a potential at widely applications due to high surface area to volume ratio. The formation mechanism of Bi_2Te_3 NSAs was proposed as well. The Bi_2Te_3 NSAs for counter electrode of CdSe QD-SSCs with the PV conversion efficiency of 1.12 % has been demonstrated. The proposed process may be used for synthesis of other NSAs using different materials such as Sb_2Te_3 and $MoSe_2$ in future.

Acknowledgements:

The research was supported by the National Science Council through grants no, NSC 101-2112-M-007-015-MY3, 101-2218-E-007-009-MY3, 102-2633-M-007-002, and the National Tsing Hua University through Grant no. 102N2022E1. Y.L. Chueh greatly appreciates the use of facility at CNMM, National Tsing Hua University through Grant no. 102N2744E1.

Supporting Information Available:

†Electronic Supplementary Information (ESI) available.

REFERENCES

[1] M. Xu, T. Liang, M. Shi, H. Chen, *Chemical Reviews* 2013, *113*, 3766.

[2] K. S. Novoselov, A. K. Geim, S. V. Morozov, D. Jiang, Y. Zhang, S. V. Dubonos, I. V. Grigorieva, A. A. Firsov, Science 2004, 306, 666.

[3] Y. Lin, T. V. Williams, J. W. Connell, The Journal of Physical Chemistry Letters 2009, 1, 277.

[4] V. Stengl, J. Henych, Nanoscale 2013, 5, 3387.

[5] D. Teweldebrhan, V. Goyal, A. A. Balandin, Nano Letters 2010, 10, 1209.

[6] Z. Ding, S. K. Bux, D. J. King, F. L. Chang, T. -H. Chen, S. -C. Huang, R. B. Kaner, Journal of Materials Chemistry 2009, 19, 2588.

[7] T. Chen, G. H. Guai, C. Gong, W. Hu, J. Zhu, H. Yang, Q. Yan, C. M. Li, Energy & Environmental Science 2012, 5, 6294.

[8] F. Tu, J. Xie, G. Cao, X. Zhao, Materials 2012, 5, 1275.

[9] R. J. Mehta, Y. Zhang, C. Karthik, B. Singh, R. W. Siegel, T. Borca-Tasciuc, G. Ramanath, Nat Mater 2012, 11, 233-240.

[10] V. Goyal, D. Teweldebrhan, A. A. Balandin, Applied Physics Letters 2010, 97, 133117.

[11] A. Balandin, K. L. Wang, Journal of Applied Physics 1998, 84, 6149.

[12] B. Qiu, X. Ruan, Applied Physics Letters 2010, 97, 183107-183103.

[13] C. -L. Chen, Y. -Y. Chen, S. -J. Lin, J. C. Ho, P. -C. Lee, C. -D. Chen, S. R. Harutyunyan, The Journal of Physical Chemistry C 2010, 114, 3385.

[14] W. Richter, C. R. Becker, physica status solidi (b) 1977, 84, 619.

[15] J. R. Drabble, C. H. L. Goodman, Journal of Physics and Chemistry of Solids 1958, 5, 142.

[16] B. -L. Huang, M. Kaviany, Physical Review B 2008, 77, 125209.

[17] W. Kullmann, J. Geurts, W. Richter, N. Lehner, H. Rauh, U. Steigenberger, G. Eichhorn, R. Geick, physica status solidi (b) 1984, 125, 131.

[18] H. J. Goldsmid, Proceedings of the Physical Society 1958, 71, 633.

[19] J. P. Fleurial, L. Gailliard, R. Triboulet, H. Scherrer, S. Scherrer, Journal of Physics and Chemistry of Solids 1988, 49, 1237-1247.

[20] Z. Tachan, M. Shalom, I. Hod, S. Ru□hle, S. Tirosh, A. Zaban, The Journal of Physical Chemistry C 2011, 115, 6162.

[21] Z. Yang, C. -Y. Chen, C. -W. Liu, C. -L. Li, H. -T. Chang, Advanced Energy Materials 2011, 1, 259.

[22] G. Sixto, M. -S. Iván, M. Lorena, G. Nestor, L. -V. Teresa, G. Roberto, J. D. Lina, S. Qing, T. Taro, B. Juan, Nanotechnology 2009, 20, 295204.

[23] M. Seol, E. Ramasamy, J. Lee, K. Yong, The Journal of Physical Chemistry C 2011, 115, 22018. [24] S. K. Mishra, S. Satpathy, O. Jepsen, Journal of Physics: Condensed Matter 1997, 9, 461.

[25] J. Nagao, E. Hatta, K. Mukasa, The 15th International Conference on Thermoelectrics, 1996, pp. 404-407.

[26] L. J. Diguna, Q. Shen, J. Kobayashi, T. Toyoda, Applied Physics Letters 2007, 91, 023116.

[27] Y. -L. Lee, Y. -S. Lo, Advanced Functional Materials 2009, 19, 604.

[28] H. Lee, M. Wang, P. Chen, D. R. Gamelin, S. M. Zakeeruddin, M Gra□tzel, M. K. Nazeeruddin, Nano Letters 2009, 9, 4221.

Table Captions

Table 1. Electrolysis parameters at various applied biases.

Applied bias (Voltage)	-2	-5	-10	-15	-20
Duration (sec.)	300	120	60	45	30

Table 2. Photovoltaic properties of QD-SSCs.

Electrode	V_{oc} (V)	J_{sc} (mA/cm^2)	FF	η (%)	Ref.
TiO_2/CdSe, Pt	0.62	7.31	0.41	1.84	This work
TiO_2/CdSe, Pt	0.65	4.65	0.31	0.90	[26]
TiO_2/CdSe, Pt	0.68	6.03	0.39	1.60	[26]
TiO_2/CdSe, Pt	0.46	8.70	0.31	1.24	[27]
TiO_2/CdSe, Pt	0.65	3.27	0.50	1.08	[28]
TiO_2/CdSe, Pt	0.61	3.93	0.49	1.19	[28]
TiO_2/CdSe, Bi_2Te_3 NSAs	0.58	6.89	0.28	1.12	This work
TiO_2/CdSe, FTO	0.57	2.20	0.14	0.18	This work

Figure captions

Figure 1. Schematics of the experiment flow chart and SEM images. (a) Bi_2Te_3 bulk. (b) three electrode system. (c) Bi_2Te_3 NSAs. (d) SEM image of Bi_2Te_3 NSAs and a higher magnification image (inset).

Figure 2. Material analysis for Bi_2Te_3 NSAs. (a) XRD spectra of Bi_2Te_3 bulks w/ and w/o NSAs. (b) Raman spectra of Bi_2Te_3 nanosheet and Bi_2Te_3 bulk. (c) A TEM image of Bi_2Te_3 nanosheet. Inset shows the corresponding diffraction pattern. (d) A high resolution TEM image of Bi_2Te_3 nanosheet taken from (c).

Figure 3. Schematics of mechanism of Bi_2Te_3 NSAs. (a) Unit cell of Bi_2Te_3. (b) Formation schematics of Bi_2Te_3 NSAs at different steps and corresponding SEM images. (c) Schematics of the hydrogen ion reacts with Bi_2Te_3 and forms Bi_2Te_3 NSAs.

Figure 4. (a) Spacing distances of Bi_2Te_3 NSAs under different applied biases and (b-f) their corresponding SEM images. The top parts are low-magnification images while the bottom parts are high-magnification images

Figure 5. Electrical properties statistics of Bi_2Te_3 nanosheets and schematics of electronic device (inset).

Figure 6. J-V characteristic of CdSe QD-SSCs with three different counter electrodes (Bi_2Te_3 NSAs, pure FTO, and Pt).

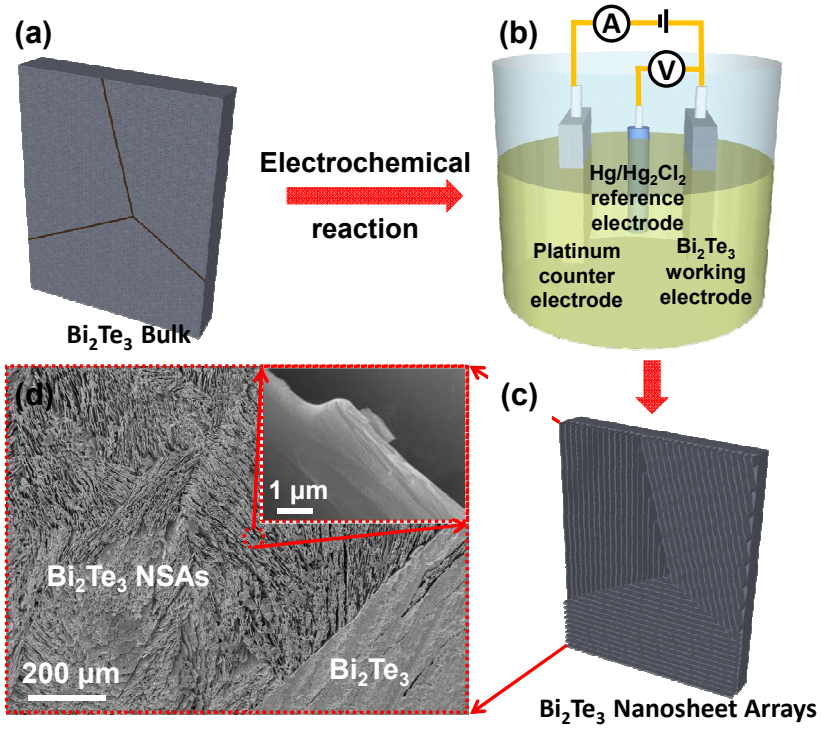

Figure 1

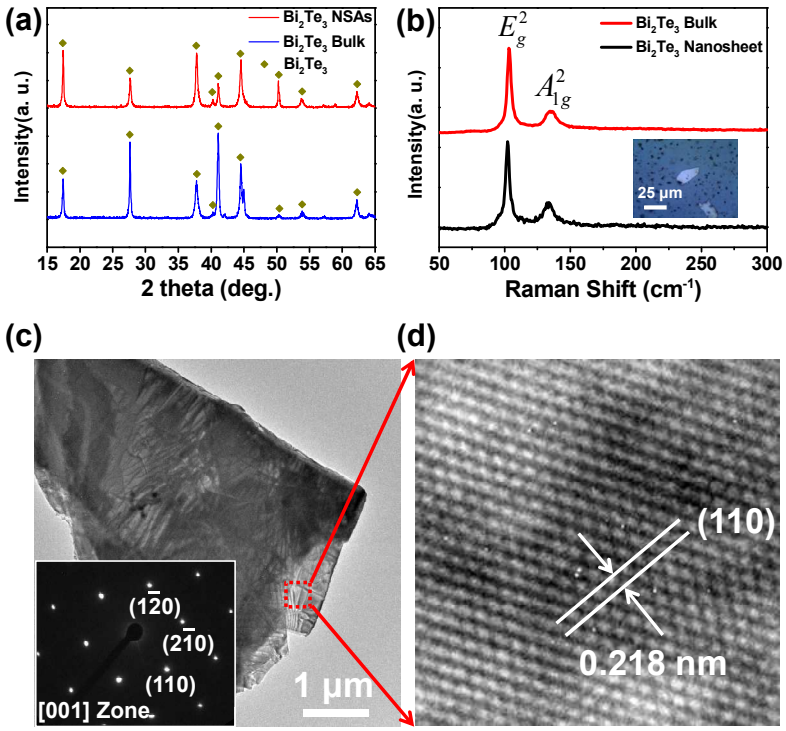

Figure 2

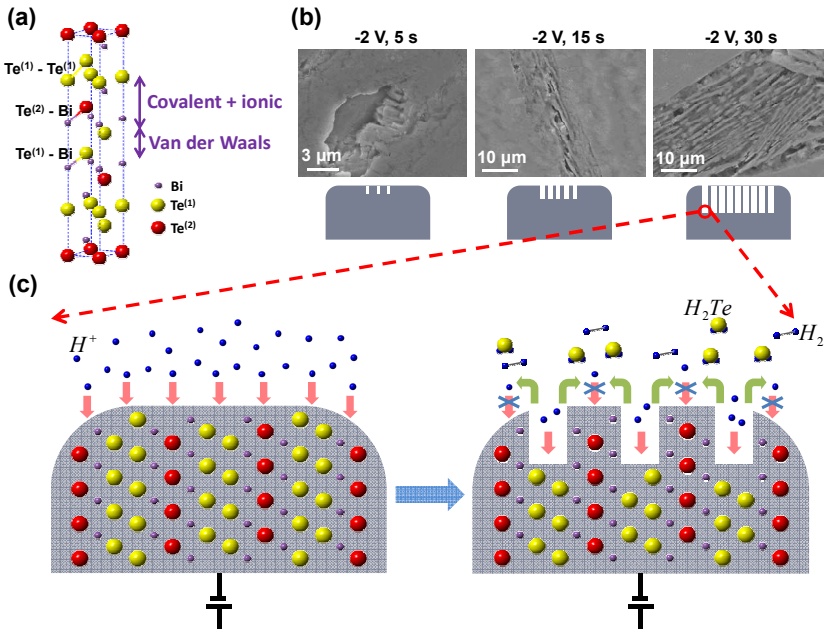

Figure 3

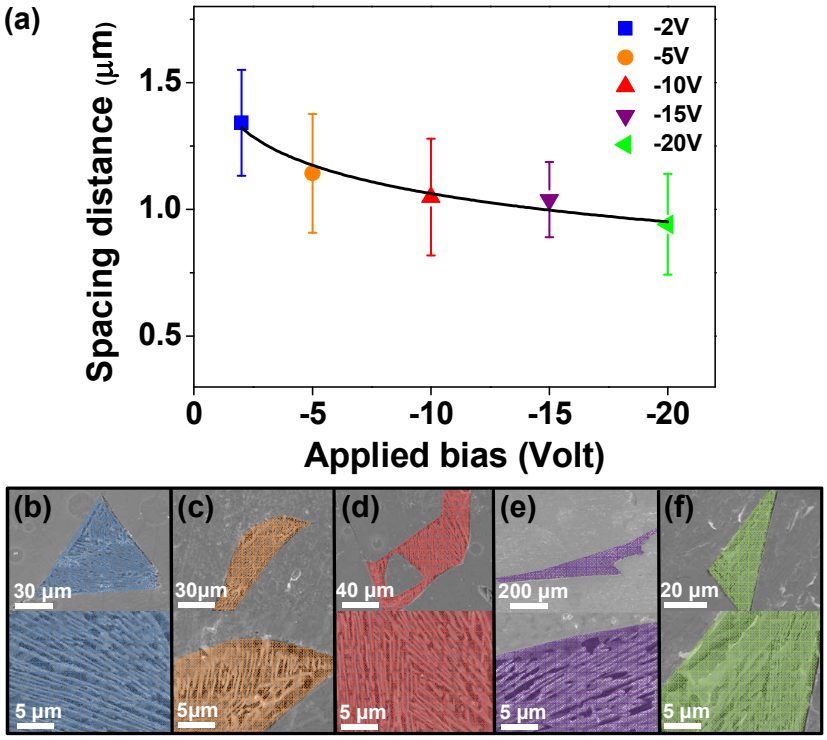

Figure 4

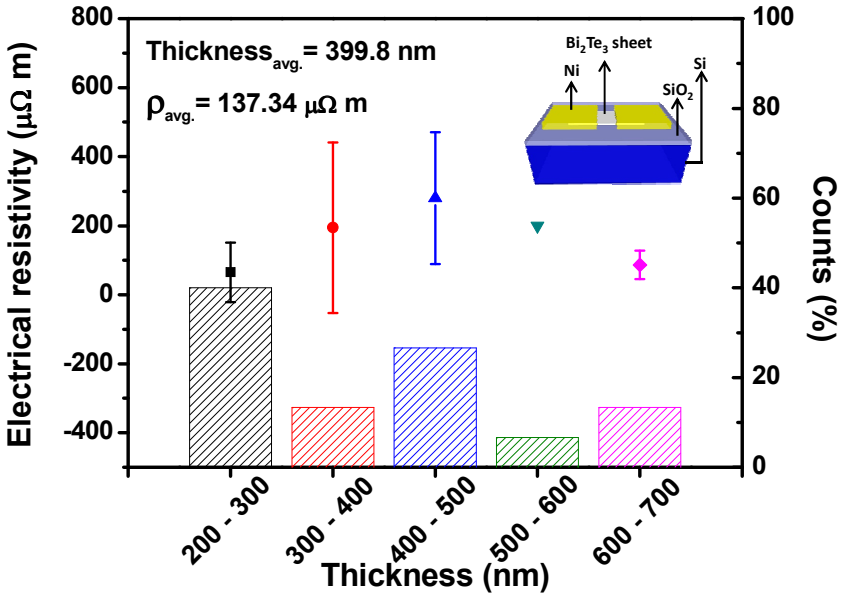

Figure 5

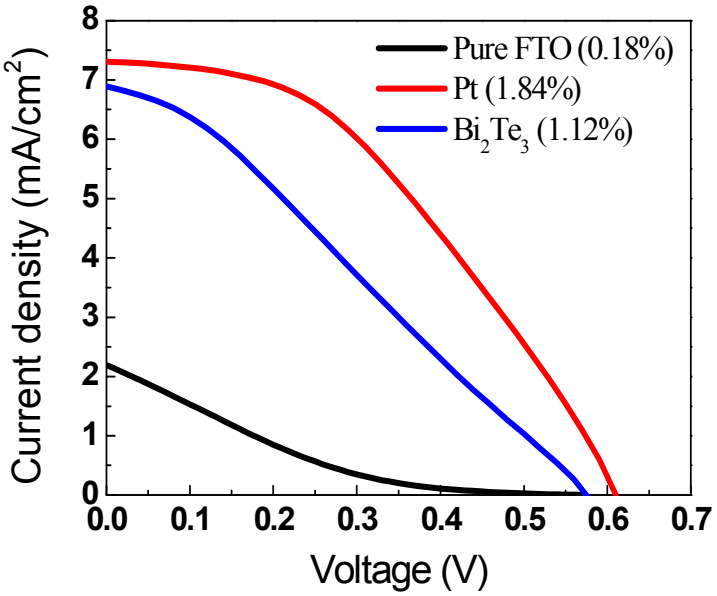

Figure 6

TOC